Journal of Alloys and Compounds 519 (2012) 9–14

Contents lists available at SciVerse ScienceDirect

Journal of Alloys and Compounds

journal homepage: www.elsevier.com/locate/jallcom

Annealing effects on the microstructure of combustion synthesized Eu^{3+} and Tb^{3+} doped Y_2O_3 nanoparticles

Srirupa T. Mukherjee[a], V. Sudarsan[a], P.U. Sastry[b], A.K. Patra[b], A.K. Tyagi[a,*]

[a] Chemistry Division, Bhabha Atomic Research Centre, Mumbai 400 085, India
[b] Solid State Physics Division, Bhabha Atomic Research Centre, Mumbai 400 085, India

ARTICLE INFO

Article history:
Received 29 May 2011
Received in revised form 23 October 2011
Accepted 24 October 2011
Available online 7 November 2011

Keywords:
Powders
Chemical preparation
Electron microscopy
X-ray methods
Optical properties
Y_2O_3

ABSTRACT

Eu^{3+} and Tb^{3+} doped Y_2O_3 powders having different Eu^{3+}/Tb^{3+} concentrations were prepared by gel-combustion process using glycine as fuel (reducing agent) and corresponding metal nitrates as oxidant, followed by annealing at 600 and 1200 °C. From XRD, SEM and TEM studies, it is inferred that for these samples, the extent of aggregation and average particle size strongly depends on the annealing temperatures. Small angle X-ray scattering (SAXS) studies on these samples revealed that the scattering intensity at large values of momentum transfer vector (Q) vary as Q^{-4}, establishing the lack of surface fractal nature as well as existence of a non-diffusive and smooth pore grain interface in both 600 and 1200 °C annealed samples. Dopant ions up to 10 at.% do not have any effect on particle/pore morphology of the samples. Improved luminescence from 1200 °C heated sample compared to 600 °C heated sample has been explained based on the difference in particle size and associated difference in the surface area.

1. Introduction

Y_2O_3 is widely used as a host matrix for various lanthanide ions and has got potential applications in fluorescent lamps, projection televisions, field emission displays and cathode-ray tubes [1–3]. The luminescence efficiency from Y_2O_3 based materials strongly depends on the physical properties of the material such as the surface morphology, crystallinity, phase-purity and distribution of activator in the matrix [4–8]. It is observed that by decreasing the grain size of host materials from macroscopic scale to nanoscale leads to many advantages. Important among them are the reduced electron penetration depth and subsequently lower excitation voltages [9], which give rise to higher luminescence efficiency and better resolution for display devices. Tb^{3+} co-doped Y_2O_3:Eu^{3+} bulk crystals are found to have improved Eu^{3+} luminescence, due to energy transfer from Tb^{3+} to Eu^{3+} ions [10]. In order to develop luminescent materials with improved luminescence characteristics for using them in various display devices, it will be of interest to synthesize and study the luminescence properties of such nano-phosphors. Among a variety of methods available for the production of nanocrystalline Y_2O_3:Ln (Ln = Eu^{3+} or Tb^{3+}) powders, the gel-combustion method (solution combustion synthesis) combine the virtues of chemical sol–gel process and low-temperature combustion process. The method is based on initial formation of a gel by thermal concentration of an aqueous solution of nitrates of desired lanthanide ions as oxidants and some organic compounds as fuels (reducing agents) followed by an auto-ignition process leading to nano-sized homogenous powder.

Jacobsohn et al. [11] have carried out detailed luminescence studies on lanthanide ions doped Gd_2O_3 nanoparticles obtained by solution combustion synthesis (SCS) method. Based on this study, the authors have inferred that the improved crystallinity and elimination of structural disorders are responsible for the improvements in the photoluminescence yield from the samples. In a related study Strek et al. [12] have investigated the size effect of the luminescence properties of Lu_2O_3:Eu nanoparticles and it is confirmed that, there exists agglomeration of Eu^{3+} in these nanoparticles. Luminescence studies on Y_2O_3:Eu nanoparticles prepared by wet chemical methods were carried out by, Polizzi et al. [13]. They have inferred that there exists considerable amount of distortion around Eu^{3+} ions in such nanoparticles. Further, it is also observed that Eu^{3+} doping do not have any effect on the morphology of the nanomaterials.

Another property of the samples prepared by gel combustion/sol–gel method is the occurrence of fractal behaviour in the sample [14–16]. Polizzi et al. [17] from the detailed X-ray scattering studies on lanthanide doped Y_2O_3 nano-particles, revealed the existence of a very porous, open microstructure with fractal scaling properties. It is also inferred that up to at least 200 nm, the particle aggregate is a mass fractal with a

---

* Corresponding author. Fax: +91 22 2550 5151.
E-mail address: aktyagi@barc.gov.in (A.K. Tyagi).

0925-8388/$ – see front matter © 2011 Elsevier B.V. All rights reserved.
doi:10.1016/j.jallcom.2011.10.080

fractal dimension, D_f, in the range of 1.6–2.0. It is known that the non radiative properties of the excited state of lanthanide ions depend on whether the host in which it is incorporated exists as three dimensional solid or as a fractal system. For example, time dependence of $^1D_2 \rightarrow {}^3H_4$ luminescence of Pr^{3+}in fluorozirconate glass, which shows fractal behaviour, follows different mechanism compared to the Pr^{3+} in a normal three dimensional solid [18]. It is also worth studying the effect of particle/pore-grain interface on the luminescence property of the nanoparticles. The present paper deals with the investigation of the nature of surface and pore-grain interface existing in Eu^{3+} co-doped Y_2O_3:Tb nanoparticles and their effect on the luminescence properties. A variety of techniques like scanning electron microscopy (SEM), transmission electron microscopy (TEM), small angle X-ray scattering (SAXS) and photoluminescence have been used to understand this. To the best of authors' knowledge this is the first time that studies in this direction are being carried out for Eu^{3+} co-doped Y_2O_3:Tb nanoparticles.

2. Experimental

All raw materials used for synthesis of nano-powder were of Analytical Reagent grade. Stoichiometric amounts of solid oxides of yttrium, europium and terbium were dissolved in aqueous nitric acid. Required amount of glycine was added by keeping nitrate to glycine ratio 1:2. The solution was slowly heated at ~100 °C on a hot plate to form a clear glassy gel by removal of excess moisture. This gel on further heating at ~200 °C was converted to a white fluffy powder. The powder was calcined at 600 °C for 30 min and 1200 °C for 1 h. SAXS, XRD, SEM and TEM experiments were performed on the powder samples to obtain information on particle morphology/surface and size.

X-ray diffraction measurements were carried out at room temperature using a Philips X-ray diffractometer using Cu-K$_\alpha$ radiation. The crystallite sizes were calculated using Scherrer's formula. Small amount of powder was dispersed on a double-sided carbon tape for recording SEM images. The images were taken on a Tescan Vega MV 23007/40, instrument using an accelerating voltage of 20 kV. SEM images were captured using a secondary electron detector. SAXS measurements were conducted using a SAXS setup mounted on a 12 kW Rigaku rotating anode X-ray generator. Nickel filter was used to obtain monochromatic Cu-K$_\alpha$ radiation ($\lambda = 0.154$ nm) for the purpose. Angular distribution of SAXS intensity was measured over an angular range of 0.05–2.5° by automated sequential mode of data collection. A scintillation counter was used for detecting the scattered X-ray intensity. All luminescence measurements were carried out at room temperature using Hitachi F-4500 instrument with a 150 W Xenon lamp as the excitation source. Around 50 mg of the sample was uniformly spread in between two quartz plates and mounted inside the sample chamber of the instrument. The parameters like slit width (3 nm), dwell time (0.2 s) and number of scans (1) were kept constant for all the samples, so that comparison of the relative intensities of peaks in the emission spectra of different samples can be done. Lifetime values for the $^5D_0$ level of Eu^{3+} ions were measured at room temperature using an Edinburgh Instruments' FLSP 920 system, having a 60 W microsecond flash lamp as the excitation source. All emission spectra were corrected for the detector response. Fourier transformed infrared (FTIR) spectra were recorded using a Bomem MB102 FT-IR spectrometer with a resolution of 4 cm^{-1}. Around 5 mg of the nanoparticles were mixed with 50 mg of dry KBr powder, ground well and made into the form of a thin pellet. The pellet is mounted inside the sample chamber of the IR machine prior to the FTIR measurements. Immediately after recording the IR spectrum of samples, IR pattern of the blank KBr was also recoded and subtracted from that of the sample. Surface area of the samples were measured based on BET method using Autosorb machine, with nitrogen as the adsorbing gas.

3. Results and discussion

X-ray diffraction patterns carried out at room temperature on all the Eu^{3+}–Tb^{3+} doped Y_2O_3 samples heated at 600, 900 and 1200 °C revealed the existence of single phase cubic structure of yttria. The average crystallite sizes were estimated from the line width of the XRD peaks and found to be in the range of 20–25 nm for 600 °C annealed, 30–34 nm for 900 °C annealed and 40–43 nm for 1200 °C annealed samples. As the crystallite sizes are significantly different for 600 and 1200 °C heated samples, SEM, TEM and SAXS studies were carried out only for 600 and 1200 °C heated samples. Representative XRD patterns for both 600 and 1200 °C heated samples along with variation of lattice parameters as a function of composition for both the samples are shown in Fig. 1. Slight reduction in the line width of 1200 °C calcined sample compared to 600 °C heated sample has been attributed to the increase in the crystallite size due to sintering by annealing. Improved signal to noise ratio of the 1200 °C heated sample compared to 600 °C heated ones is attributed to the improved crystallinity of the former sample compared to the latter. Based on the least square fitting of the diffraction peaks the lattice parameters have been calculated for both 600 and 1200 °C heated samples and the values are found to be slightly higher for the 1200 °C heated samples compared to 600 °C heated samples. Further, the lattice parameter has been found to increase systematically with increase in Eu^{3+} content in the sample. A linear variation of lattice parameters indicates a random distribution of lanthanide ions in Y_2O_3 host as predicted by the Vegard's law. Fig. 2 shows the SEM image obtained from Y_2O_3:2%Eu^{3+},8%Tb^{3+} nanoparticles heated at 600 °C. The images very clearly demonstrate that the sample is highly porous with pore sizes ranging from around 500 to 2000 nm. Wide pore size distribution existing in the sample has been attributed to profuse evolution of gas, taking place during the auto-ignition step of synthesis.

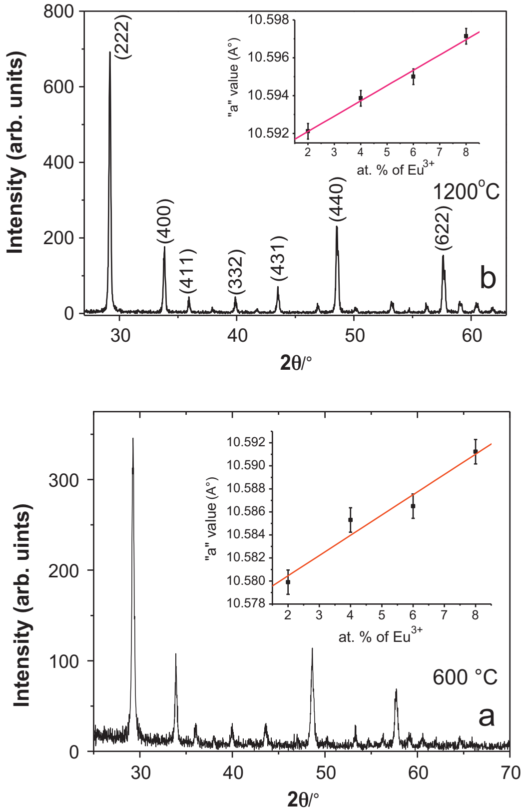

Fig. 1. XRD pattern of Y_2O_3:2%Eu^{3+},8%Tb^{3+} nanoparticles heated at (a) 600 °C and (b) 1200 °C. Inset shows the variation of lattice parameter with increase in Eu^{3+} concentration in the lattice.

In order to understand, the particles size distribution and the extent or the nature of grain growth among the nanoparticles brought about by the annealing temperatures namely 600 and 1200 °C, TEM images were recorded for both the samples and are shown in Fig. 3(a and b). For 600 °C heated sample, particle (grain) sizes are smaller, having a size range approximately 25–150 nm and they are arranged in a chain like fashion. For 1200 °C heated sample particle/grain size has got a broad distribution and is in the range of 100–400 nm. As expected sample annealed at 600 °C undergoes aggregation to a lesser extent compared to 1200 °C heated sample. Based on TEM studies, it is inferred that significant change in particle/grain size and shape take place with increase in heat treatment temperature from 600 to 1200 °C. Increase in particle size reduces the surface area of the sample leading to the decrease in

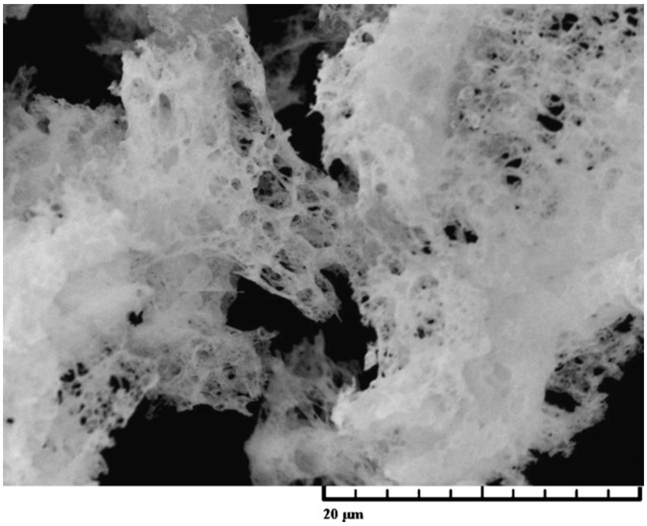

Fig. 2. SEM micrograph of Y_2O_3:2%Eu^{3+},8%Tb^{3+} nanoparticles heated at 600 °C.

sample sensitivity toward moisture [7,8]. Such an effect is expected to improve the emissive properties of the sample.

In all the above studies, no information is obtained regarding the surface structure of the nanoparticles (grains), interface between the grains and their behaviour under different annealing temperatures, particularly at length scales less than 100 nm. In order to understand this aspect, SAXS measurements were carried out on the samples annealed at 600 and 1200 °C. Both XRD and SAXS respond to small-scale fluctuations of the electronic density within the scattering medium. The difference between XRD and SAXS is that XRD is sensitive to the inter-atomic distances roughly within the range 0.05–1 nm, whereas SAXS provides information about the electronic density fluctuations in the linear size range from 1 nm to 100 nm. In SAXS experiments the scattered intensity is measured as a function of Q, the momentum transfer vector. This parameter depends on the wavelength of the incident radiation and the angle at which the scattered radiation is detected and is reciprocally related to the spatial distances probed within the sample. The X-ray momentum transfer vector is defined by

$$Q = 4\pi \frac{\sin(\theta/2)}{\lambda} \tag{1}$$

where θ is the angle between the incident and scattered radiation and λ is the wavelength of the incident radiation [19]. In the present study SAXS data were recorded over the scattering wave vector (Q) range of 0.036–1.7 nm^{-1}. The SAXS profiles were corrected for absorption and slit height-smearing effects before analyzing the data [19]. SAXS profiles of powder samples annealed at same temperature match very nearly with each other. This indicates that the dopants have negligible effect on particle/pore morphology. Fig. 4(a and b) shows the representative SAXS profiles of Y_2O_3:Eu^{3+},Tb^{3+} nanoparticles annealed at 600 and 1200 °C. A smooth fall of intensity with no peak and oscillations in the recorded Q regime of the profiles indicates scattering from non-interacting and polydisperse system of particles/pores. For such systems scattering intensity can be expressed by Debye–Bueche function, given by Eq. (2):

$$I(Q) = C(1 + a^2Q^2)^{-2} \tag{2}$$

The scaling parameter C is independent of Q but depends on sample parameters like scattering contrast and number density of particles and instrument parameters like slit size and incident flux. The parameter 'a' is average size of the inhomogeneities in the

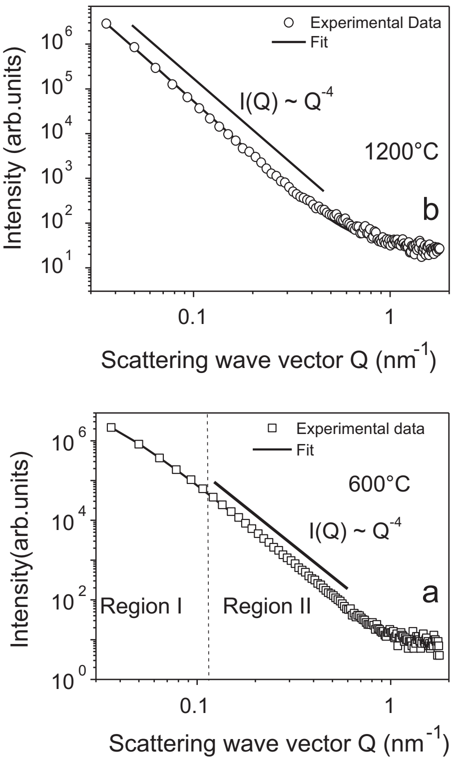

Fig. 4. SAXS profiles of the powder samples heated at (a) 600 °C and (b) 1200 °C.

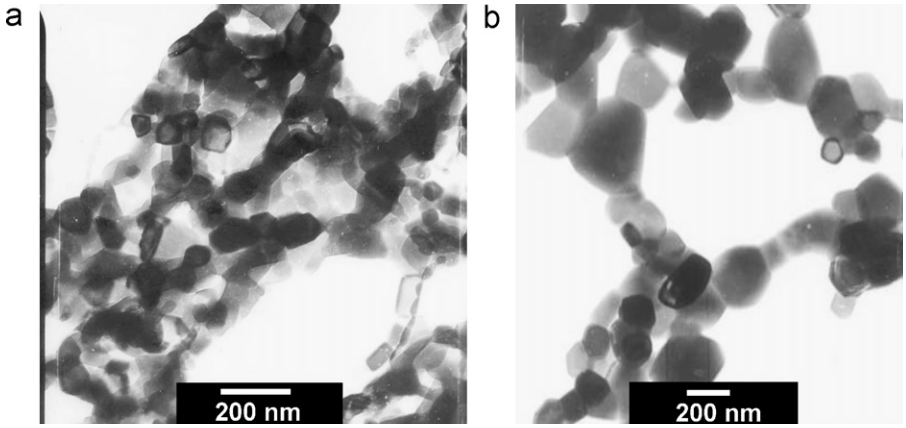

Fig. 3. TEM images of (a) 600 °C and (b) 1200 °C heated samples.

sample. Experimental SAXS data fit well with the scattering intensity function given by Eq. (2). From these results, it is inferred that the scattering is taking place from three-dimensional volumes having shapes like spheres, cubes or fat discs having aspect ratio between one and two. Further it is also clear that the particles/pores are randomly distributed in the irradiated sample volume [20–23]. For 600 °C heated sample, variation of the scattering intensity can be divided into two regions. The region 1 (i.e. for low Q values) scattering intensity decreases relatively slowly with increasing Q; whereas in the region 2 (high Q region) scattering intensity decreases faster than region 1 and follows Q^{-4} variation. In the case of 1200 °C heated sample the SAXS intensity increases monotonically with decreasing Q and follows a Q^{-4} dependence over a wide range of Q values. This behaviour of 1200 °C heated sample indicates that the average size of the particles/pores is large and is beyond the sensitivity of the instrument. The Q^{-4} dependence of scattering corresponds to the so-called Porod's law, which indicates that the surfaces of the crystallites are very smooth and there exists a non-diffusive boundary between grains and pores. According to the concept of surface fractal, scattering intensity $I(Q)$ obeys a power law formula $I(Q) \sim Q^{-N}$, where the exponent N is related to the surface fractal dimension D_s through $N = 2D - D_s$ in D-dimensional space. In three-dimensional space, for example, the value of D_s ranges from 2 to 3, corresponding to the range of N from 4 to 3. The Porod's law, $I(Q) \sim Q^{-4}$ is a particular case of surface fractal scattering [23]. It has also been shown that for particles of uniform electron density and surface area, scattering intensity at large Q is proportional to the total surface area [19]. It is also observed that the scattering profile of sample heated at 1200 °C is sharper than that of 600 °C heated sample. The observed difference in the behaviour of scattering intensity as a function of Q for 600 °C heated sample compared to 1200 °C heated sample has been attributed to the smaller size and associated larger surface area of the 600 °C annealed samples compared to the ones annealed at 1200 °C. Further, the presence of non-diffusive boundary between grains and pores for both 600 and 1200 °C heated sample confirms that no surface fractal nature is existing for these samples. In other words the nature of the surface is almost identical for both 600 and 1200 °C heated sample and surface area alone is different for these two samples.

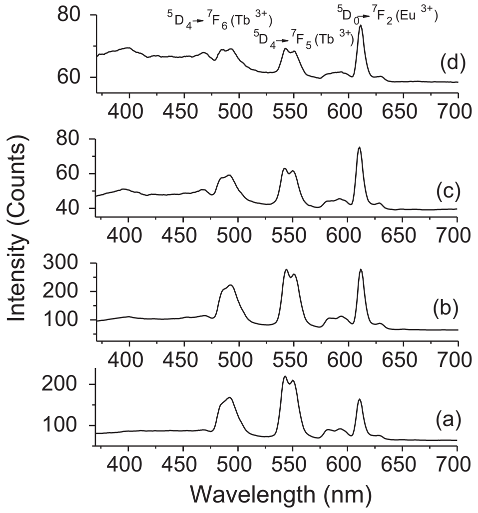

Fig. 5. Emission spectra from Eu^{3+} co-doped Y_2O_3:Tb^{3+} nanoparticles as a function of composition obtained after excitation at 287 nm for 600 °C heated samples of (a) Y_2O_3:2%Eu^{3+},8%Tb^{3+}; (b) Y_2O_3:4%Eu^{3+},6%Tb^{3+}; (c) Y_2O_3:6%Eu^{3+},4%Tb^{3+} and (d) Y_2O_3:8%Eu^{3+},2%Tb^{3+}.

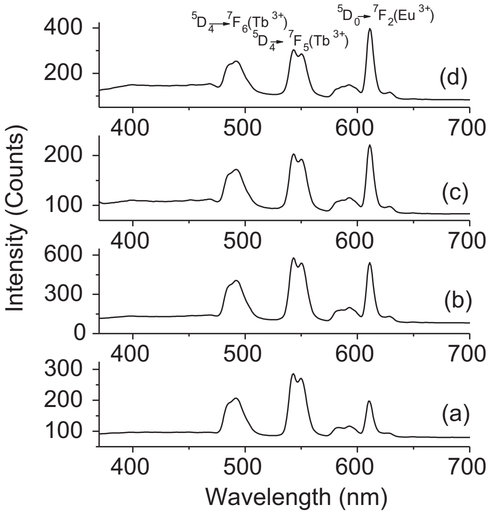

Fig. 6. Emission spectra from Eu^{3+} co-doped Y_2O_3:Tb^{3+} nanoparticles as a function of composition obtained after excitation at 287 nm for 1200 °C heated samples of (a) Y_2O_3:2%Eu^{3+},8%Tb^{3+}; (b) Y_2O_3:4%Eu^{3+},6%Tb^{3+}; (c) Y_2O_3:6%Eu^{3+},4%Tb^{3+} and (d) Y_2O_3:8%Eu^{3+},2%Tb^{3+}.

Figs. 5 and 6 show the emission spectra for Eu^{3+} co-doped Y_2O_3:Tb^{3+} nanoparticles annealed at 600 and 1200 °C as a function of composition. The corresponding excited state lifetimes of $^5D_0$ level of Eu^{3+} and $^5D_4$ level of Tb^{3+} in these samples are shown in Table 1. The spectrum is characterized by strong emission peaks around 490 and 545 nm characteristic of Tb^{3+} and 590 and 612 nm characteristic of Eu^{3+} ions. For 900 °C heated samples the intensity of luminescence (counts corresponding to the most intense peak) has been found to be almost in between that of 600 and 1200 °C heated samples. Further, the relative intensity of the peaks corresponding to both Tb^{3+} and Eu^{3+} ions varies in accordance with the variation in the relative concentration of Tb^{3+} and Eu^{3+} in the nanoparticles. Relative intensity of both 590 and 615 nm peak in the emission spectrum corresponding to all the samples has been found to be close to 1:3 ratio, suggesting that presence of Tb^{3+} along with Eu^{3+} in Y_2O_3 lattice do not have any effect on the extent of

Table 1
Characteristic lifetime and β values corresponding to the $^5D_0$ level of Eu^{3+} and lifetime components corresponding to $^5D_4$ level of Tb^{3+} in Eu^{3+} and Tb^{3+} doped Y_2O_3 nanoparticles prepared by combustion method and annealed at 600 and 1200 °C.

Sample	Lifetime values									
	$^5D_0$ level of Eu^{3+}				$^5D_4$ level of Tb^{3+}					
	600 °C		1200 °C		600 °C			1200 °C		
	τ_{ch} (ms)	β	τ_{ch} (ms)	β	τ_{fast} (μs)	τ_{ch} (ms)	β	τ_{fast} (μs)	τ_{ch} (ms)	β
Y_2O_3:2%Eu^{3+},8%Tb^{3+}	1.0	1.0	1.1	1.0	23.0	0.130	0.46	115	0.180	0.50
Y_2O_3:4%Eu^{3+},6%Tb^{3+}	1.3	0.96	1.1	0.92	7.6	0.97	0.32	91	0.130	0.44
Y_2O_3:6%Eu^{3+},4%Tb^{3+}	1.2	0.87	1.1	0.89	4.9	0.026	0.30	74	0.087	0.40
Y_2O_3:8%Eu^{3+},2%Tb^{3+}	1.3	0.84	1.3	0.89	5	0.011	0.25	7	0.020	0.21

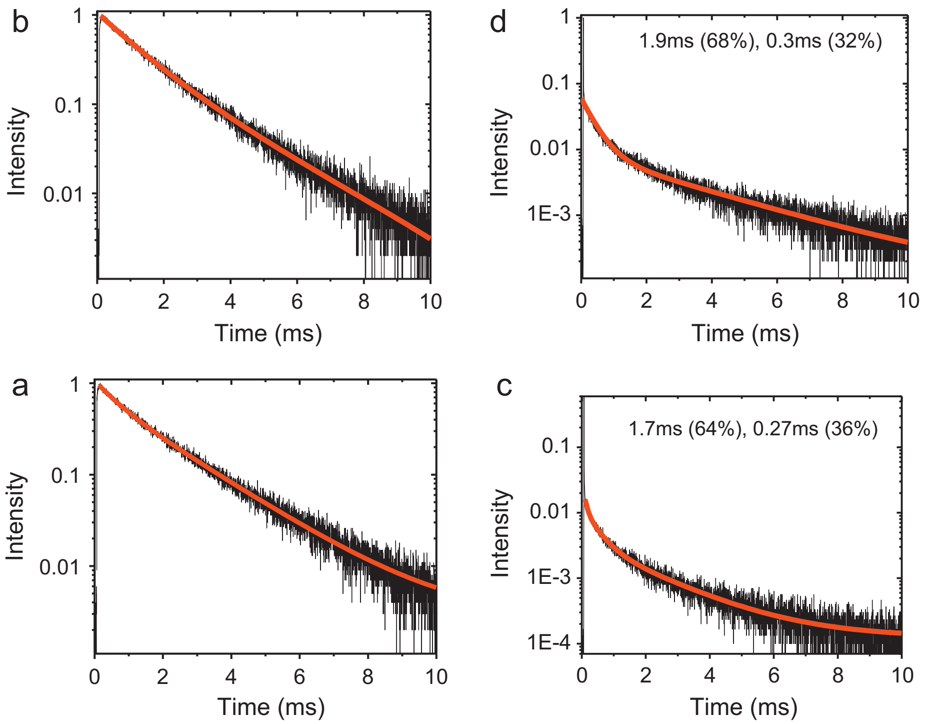

Fig. 7. Decay curves corresponding to $^5D_0$ level of Eu^{3+} in Y_2O_3:8%Eu^{3+},2%Tb^{3+} nanoparticles heated at (a) 600 °C and (b) 1200 °C. The corresponding curves for $^5D_4$ level of Tb^{3+} from the sample heated at 600 and 1200 °C are shown in (c and d), respectively.

distortion around Eu^{3+} ions. The excited sate corresponding to the $^5D_0$ level of Eu^{3+} can be fitted to a stretched exponential model [24] (Fig. 7(a)) based on Eq. (3)

$$I(t) = I_0 e^{-(t/\tau_{ch})^{\beta}} \qquad (3)$$

where $I(t)$ is the intensity at any time "t" and I_0 the intensity at the beginning of the decay measurements (intensity at zero time). The parameter "τ_{ch}" is the characteristic lifetime for decay of the excited state and "β" represents the degree to which the measured decay deviates from purely exponential decay. A "β" value of unity corresponds to purely exponential decay. The "β" parameter is a measure of the extent of energy transfer coupling between different excited sates. As Eu^{3+} concentration increases in Y_2O_3 host, the "β" value corresponding to the decay of $^5D_0$ level of Eu^{3+} from both 600 and 1200 °C is annealed samples slightly decreases as can be seen from Table 1. This understandable as the increase in Eu^{3+} concentration is associated with increase in the extent of non-radiative decay of the excited states, due to interactions like, dipole–dipole, cross relaxations, etc. However this is not very much reflected in the characteristic lifetime (τ_{ch}) values, as it remained more or less same for all the samples and are in the range of 1.2–1.3 ms. Possible reason for the comparable values of characteristic lifetime can be energy transfer from Tb^{3+} to Eu^{3+} as well as the averaging effect of the slower and faster decay time components.

The $^5D_4$ level of Tb^{3+} in these samples has been found to decay initially with a fast decay time of few microseconds. This is followed by a stretched exponential decay similar to that observed for $^5D_0$ level of Eu^{3+}. Representative decay curves corresponding to the samples heated at 600 and 1200 °C are shown in Fig. 7(c and d). The values of β and τ_{ch} obtained from fitting of the decay curves with stretched exponential model along with the decay time characteristic of the fast decay component is given in Table 1. The lifetime value of the fast decay component is found to be higher for the 1200 °C hated sample compared to 600 °C hated ones and this is due to the reduction in the surface hydroxyl groups brought about by the increase in annealing temperatures. The values of β are significantly lower for the $^5D_4$ level of Tb^{3+} compared to $^5D_0$ level of Eu^{3+} and this is understandable as there exists energy transfer from Tb^{3+} to Eu^{3+} ions in these samples. As the Eu^{3+} concentration increases at the expense of Tb^{3+}, the extent of self quenching between the Tb^{3+} species decreases but there exists increased extent of energy transfer between Tb^{3+} and Eu^{3+} ions due to the increased number of Eu^{3+} ions around Tb^{3+}. This is reflected in the corresponding β and τ_{ch} values.

Even though from SAXS studies, it is confirmed that nature of the surface is same for both 600 and 1200 °C annealed samples, the surface area is expected to be quite different for these samples as they are subjected to different annealing temperatures. This is clear from the measured surface area values of a representative sample of Y_2O_3:2%Eu^{3+},8%Tb^{3+} nanoparticles subjected to annealing at 600, 900 and 1200 °C. The values are found to be 31.6, 21.8 and 5.0 m^2/g for annealing temperatures 600, 1000 and 1200 °C, respectively. Decrease in surface area with increase in annealing temperatures has been attributed to the aggregation of small particles resulting in the formation of bigger particles. Higher surface area of the particles obtained at 600 °C heated sample makes it more susceptible for moisture and CO_2 absorption as compared to the 1200 °C heated sample. Vibration of surface carbonate and hydroxyl groups can significantly quench the excited state of lanthanide ions. This leads to the poor luminescence characteristics for 600 °C heated sample compared to 1200 °C heated sample. This is clear from the lower excited state lifetimes of 600 °C heated sample compared to 1200 °C heated ones. This aspect is further confirmed by the IR patterns of the 600 and 1200 °C heated samples shown in Fig. 8. The stretching and bending vibrations of the surface OH groups, around 3462 cm^{-1} and 1500 cm^{-1}, respectively, have got reduced intensity in 1200 °C heated sample compared to 600 °C heated samples. Further, the peak corresponding to Y–O vibrations around 400 cm^{-1} also got slightly reduced in 1200 °C heated sample compared to the 600 °C heated ones. Both 600 and 1200 °C heated samples contain unburned organic species as is clear from the C–H stretching

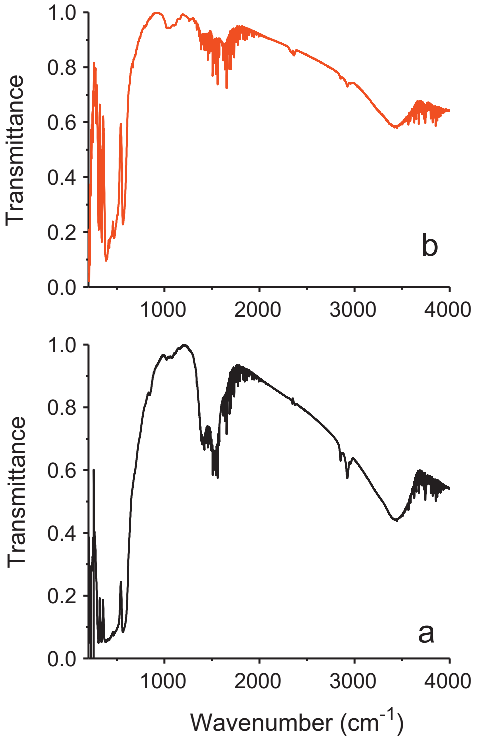

Fig. 8. IR spectra of Y_2O_3:2%Eu^{3+},8%Tb^{3+} nanoparticles annealed at (a) 600 °C and (b) 1200 °C.

vibrations observed around 2900 cm^{-1} in Fig. 8(a and b). However its concentration is much smaller in 1200 °C heated samples compared to 600 °C heated ones. In order to confirm the fact that the decrease in the intensity of the peak due to OH group vibrations, is not due to the decrease in intensity of Y–O vibrational peaks in 1200 °C heated sample, the relative ratios of the intensity of the peaks at 3462 cm^{-1} (characteristic of the OH groups) and that around 400 cm^{-1} (characteristic of the Y–O stretching vibrations) have been estimated from the IR patterns of both 600 and 1200 °C heated samples. For 600 °C heated sample the ratio of the relative intensities of peaks corresponding to Y–O and OH linkages are in the ratio 1:0.50 where as for 1200 °C heated sample the ratio is 1:0.40. These values very clearly demonstrate that OH group concentration is less in 1200 °C hated sample compared to 600 °C heated sample. Thus the IR results establish that the lesser extent of surface hydroxyl groups present with 1200 °C heated sample is indeed responsible for its improved luminescence properties compared to 600 °C heated samples.

Generally surface fractal behaviour is observed in combustion/sol–gel synthesized nanomaterials as reported by Benedetti et al. [14] and Zeng et al. [15] and such behaviour is known to significantly affect the luminescence properties of the lanthanide ions doped materials. However in the present study, SAXS experiments on both 600 and 1200 °C heated samples very clearly demonstrate that no surface fractal behaviour is existing for the samples instead there exist smooth non-diffusive boundary between pores and grains in the sample. The surface area is lower for 1200 °C heated samples compared to 600 °C heated ones as revealed by the sharper scattering profile for 1200 °C heated ones compared to 600 °C heated sample and this is in accordance with our expectations. Thus combining SAXS, luminescence and IR studies on the samples annealed at 600 and 1200 °C, it is inferred that reduced surface area and associated decrease in the relative concentration of surface hydroxyl groups in 1200 °C heated sample is responsible for its improved luminescence.

4. Conclusions

Based on XRD, SEM and TEM studies on Y_2O_3:Eu^{3+},Tb^{3+} nanoparticles annealed at different temperatures, it is concluded that, in these samples there exist significant aggregation of nanoparticles, sizes of which increase with increasing annealing temperatures. SAXS studies have confirmed that nature of the surface is almost same for both 600 and 1200 °C heated samples. Even though the powders are fluffy, no fractal behaviour is observed for the aggregates. The small angle X-ray scattering intensity curves at larger momentum transfer vector follows Porod's law indicating the existence of smooth and non-diffusive interface in these samples. Larger surface area of 600 °C heated sample compared to the 1200 °C heated sample leads to the higher extent of moisture and CO_2 absorption by the former sample compared to the latter. Vibrations of surface hydroxyl groups which are present to a higher extent in 600 °C heated samples compared to 1200 °C samples lead to increased quenching of the excited state of lanthanide ions, leading poor luminescence from 600 °C heated sample compared to 1200 °C heated sample.

References

[1] K.Y. Jung, C.H. Lee, Y.C. Kang, Mater. Lett. 59 (2005) 2451.
[2] M. Nichkova, D. Dosev, S.J. Gee, B.D. Hammock, I.M. Kennedy, Anal. Chem. 77 (2005) 6864.
[3] L. Ozawa, M. Itoh, Chem. Rev. 103 (2003) 3835.
[4] T.K. Anh, L.Q. Minh, N. Vu, T.Y. Huong, N.T. Huong, C. Barthou, W. Strek, J. Lumin. 102–103 (2003) 391.
[5] S. Ray, P. Pramanik, A. Singha, A. Roy, J. Appl. Phys. 97 (2005) 943121.
[6] P.K. Sharma, M.H. Jilavi, R. Nass, H. Schmidt, J. Lumin. 82 (1999) 187.
[7] S. Mukherjee, V. Sudarsan, R.K. Vatsa, S.V. Godbole, R.M. Kadam, U.M. Bhatta, A.K. Tyagi, Nanotechnology 19 (2008) 3257041.
[8] V. Sudarsan, F.C.J.M. van Veggel, R.A. Herring, M. Raudsepp, J. Mater. Chem. 15 (2005) 1332.
[9] J. Dhanraj, R. Jagananthan, T.R.N. Kutty, C.H. Lu, J. Phys. Chem. B 105 (2001) 11098.
[10] T.K. Anh, T. Ngoc, P. Thunga, V.T. Bich, P. Long, W. Strek, J. Lumin. 39 (1988) 215.
[11] L.G. Jacobsohn, S.C. Tornga, B.L. Bennett, R.E. Muenchausen, O. Ugurlu, T.K. Tseng, J. Choi, P.H. Holloway, Radiat. Meas. 45 (2010) 611.
[12] W. Strek, E. Zych, D. Hreniak, J. Alloys Compd. 344 (2002) 332.
[13] S. Polizzi, M. Battagliarin, M. Bettinelli, A. Speghini, G. Fagherazzi, J. Mater. Chem. 12 (2002) 742.
[14] A. Benedetti, G. Fagherazzi, P. Riello, Y.W. Zeng, J. Appl. Crystallogr. 26 (1993) 717.
[15] Y.W. Zeng, P. Riello, A. Benedetti, G. Fagherazzi, J. Non-Cryst. Solids 185 (1995) 78.
[16] G. Fagherazzi, S. Polizzi, M. Bettinelli, A. Speghini, J. Mater. Res. 15 (2000) 586.
[17] S. Polizzi, G. Fagherazzi, M. Battagliarin, M. Bettinelli, A. Speghini, J. Mater. Res. 16 (2001) 146.
[18] J.L. Rousset, M. Ferrari, E. Duval, A. Boukenter, C. Mai, S. Etienne, J.L. Adam, J. Non-Cryst. Solids 111 (1989) 238.
[19] A. Guinier, G. Fournet, Small-angle Scattering of X-rays, John Wiley and Sons Inc., New York, 1955.
[20] P.W. Schmidt, R. Hight Jr., Acta Crystallogr. 13 (1960) 480.
[21] P. Debye, A.M. Bueche, J. Appl. Phys. 20 (1949) 518.
[22] P. Debye, H.R. Anderson Jr., H. Brumberger, J. Appl. Phys. 28 (1957) 679.
[23] J.E. Martin, A.J. Hurd, J. Appl. Crystallogr. 20 (1987) 61.
[24] J.K. Krebs, Z.J. Barninger, J. Lumin. 130 (2010) 1305.